

Ni-Induced Layer Exchange of Multilayer Graphene on Plastic Substrate for Flexible Rechargeable Battery Anode

Hiromasa Murata^{1,2}, Takashi Suemasu¹, and Kaoru Toko¹

¹Institute of Applied Physics, University of Tsukuba, Tsukuba, Ibaraki 305-8573, Japan

²JSPS Research Fellow, Chiyoda, Tokyo 102-0083, Japan

Phone: +81-29-853-5472, E-mail: s1830090@s.tsukuba.ac.jp

Abstract

Ni-induced layer exchange (LE) growth of multilayer graphene (MLG) anode structures at low temperature and their operation is investigated in this study. The MLG is synthesized at 350 °C and exhibits the best anode characteristics as a low-temperature formed carbon film.

1. Introduction

All-solid-state batteries have excellent characteristics, such as high energy and power density, good capacity retention for thousands of discharge/charge cycles, and high safety. The ability to synthesize thick MLGs on plastics, which are the most common, light substrates, suggests the possibility of incorporating all-solid-state batteries into arbitrary flexible devices.

Metal-induced LE is a powerful method for synthesizing high-quality uniform MLGs directly on insulators at low temperatures [1-9]. This study investigates the thickness control of MLG and the self-organization of the MLG on a Ni-electrode structure on a plastic substrate using inverted LE with a Ni catalyst.

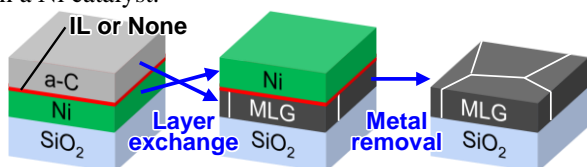


Fig. 1. Schematic of the sample preparation procedure.

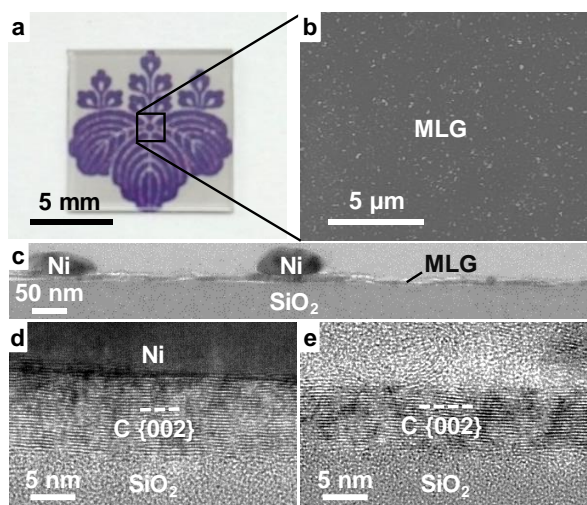


Fig. 2. (a) Photograph and (b) SEM image of the sample for $t = 5$ nm without IL after Ni removal. Characterization of the cross-section of the sample for $t = 10$ nm without the IL before Ni removal. (c) Bright-field TEM image. High-resolution lattice images of the MLG layer showing (d) a Ni-contacted region and (e) a non-Ni-contacted region.

2. Experimental Procedures

The schematic of sample preparation procedure is shown in Fig. 1. First, we investigate the thickness control of MLG. Ni films (thickness, 5–200 nm) were prepared on SiO₂ glass substrates. The thickness of the initial Ni layer determines the resulting MLG thickness, t , after LE. Subsequently, AlO_x interlayer (IL) (thickness, 1 nm) and a-C thin films were prepared, wherein the thickness ratio of C:Ni = 3:2. The IL suppresses the nucleation of the MLG, resulting in enlargement of MLG grains. For comparison, we prepared the samples without the IL. The samples were annealed at 800 °C for 1 h. Then, we investigate the low-temperature synthesis of MLG anode structures (Fig. 4(a)) and their operation. 100-nm-thick SiO₂, a-C, and Ni layers were sequentially prepared on a polyimide film (thickness, 30 μm) and Mo foil (thickness, 50 μm). The Mo foil was used instead of the polyimide film for electrochemical measurements. The samples were annealed at 350 °C for 3 h. Coin-type cells were fabricated from the MLG on the Ni (each 100 nm thick), a pure Li metal foil, and a separator (Celgard 2400), immersed in an electrolyte. The electrolyte was 1 mol L⁻¹ LiPF₆ in ethylene carbonate (EC)/diethyl carbonate (DEC) (1:1 in volume).

3. Results and Discussion

For all samples ($t = 5$ –200 nm), MLG layers were formed on the substrate via LE. As representatively shown in Fig. 2(a), thin MLG layers ($t \leq 10$ nm) exhibits transparency. The SEM image in Fig. 2(b) shows that although the MLG layer has submicron-size voids, it covers nearly the entire substrate. We note the Ni concentration in the MLG layer is below the detection limit of EDX (~1%).

Fig. 2(c) also shows the MLG formed on the entire substrate. Fig. 2(d) and 2(e) show {002} oriented MLG forms on the SiO₂ substrate in both the Ni-contacted and non-Ni-contacted regions.

Fig. 3 shows the electrical properties of the MLG strongly depend on t , and with or without the IL. Fig. 3(a) shows the carrier concentration of the MLG decreases with the increase

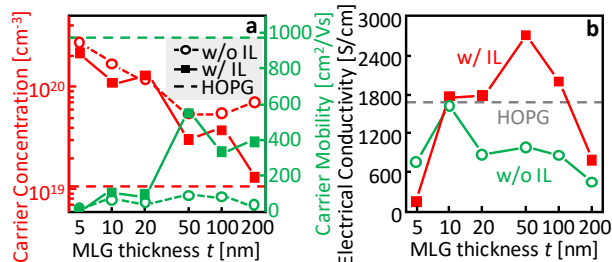


Fig. 3. Electrical properties of the MLG layers after Ni removal as a function of t . (a) Carrier concentration and carrier mobility. (b) Electrical conductivity.

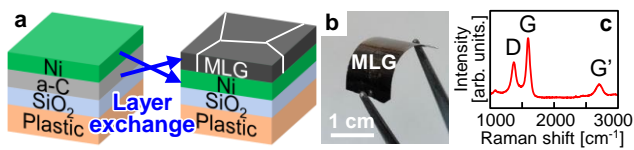


Fig. 4. (a) Schematic of the sample preparation procedure. (b) Photograph and (c) Raman spectrum of the resulting sample.

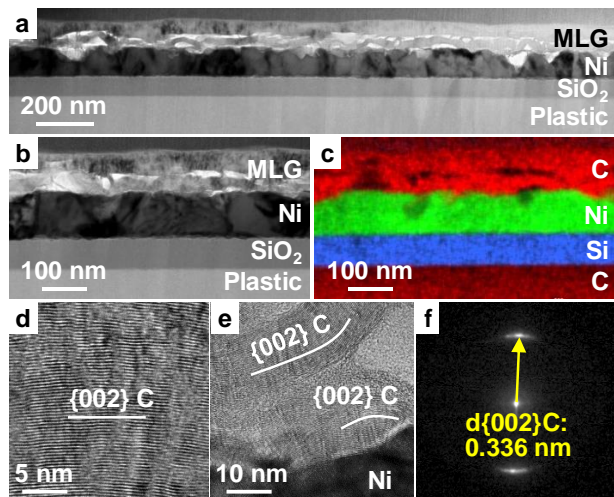


Fig. 5. Cross-sectional TEM characterization of the plastic sample. (a) Low- and (b) high- magnification bright-field TEM images. (c) EDX elemental mapping. High-resolution lattice images of the (d) upper and (e) lower MLG layers. (f) SAED pattern, taken from the region including the Ni and MLG layers.

of t and approaches the value of a highly oriented pyrolytic graphite (HOPG) with a low mosaic degree of 0.4° , especially for the sample with the IL. Fig. 3(a) also shows the carrier mobility dramatically increases for the $t \geq 50$ nm samples with the IL. The carrier mobility exhibits the maximum value of $550 \text{ cm}^2/\text{Vs}$ for the $t = 50$ nm sample with the IL, which is the highest Hall mobility among MLGs directly formed on an insulator. Fig. 3(b) shows the behavior of the electrical conductivity reflects that of the carrier mobility. The electrical conductivity exhibits the maximum value of 2700 S/cm for the $t = 50$ nm sample with the IL, which exceeds that of the HOPG synthesized at 3000°C or higher.

As shown in Fig. 4(b), the sample remains highly flexible even after annealing. The Raman spectrum exhibits D, G, and G' peaks corresponding to the graphitic structure, indicating LE occurs between Ni and a-C films.

Fig. 5(a)–(c) indicate that the MLG/Ni stacked structure was formed on the substrate via inverted LE between the Ni and a-C layers. The selected-area electron diffraction (SAED) pattern in Fig. 5(f) shows the spots corresponding to the $C\{002\}$ planes in the MLG. Thus, the MLG/Ni anode structure self-organized on the flexible plastic substrate using low-temperature inverted LE.

Fig. 6(a) shows a cathodic peak at 0.06 V , corresponding to the Li insertion into the MLG. The MLG shows the clear charge/discharge operation during 100 cycles in Fig. 6(b). At the current density of $6.7 \mu\text{A cm}^{-2}$, the discharge capacity is $6.2 \mu\text{Ah cm}^{-2}$ after 100 cycles (Fig. 6(c)), which is 77% of the initial discharge capacity ($8.0 \mu\text{Ah cm}^{-2}$). The coulombic efficiency reaches approximately 99% after 100 cycles. The rate performance shows that the capacity at $\leq 13 \mu\text{A cm}^{-2}$ is

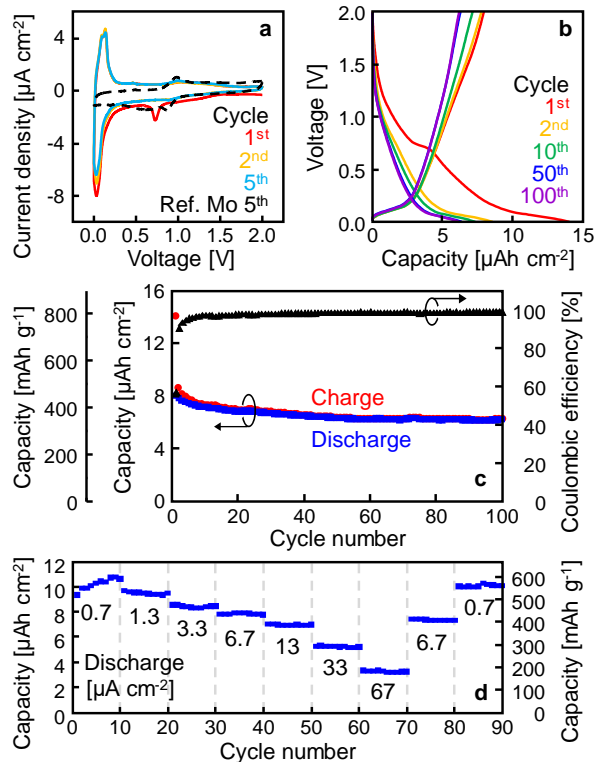


Fig. 6. Electrochemical characteristics of the MLG anode in a coin-type cell. (a) Cyclic voltammogram at a scan rate of $50 \mu\text{Vs}^{-1}$. (b) Galvanostatic charge/discharge cycles measured at a current rate of $6.7 \mu\text{A cm}^{-2}$. (c) Charge/discharge capacities and coulombic efficiency as a function of cycle number. (d) Current-rate testing at various current densities ($0.7\text{--}67 \mu\text{A cm}^{-2}$), every 10 cycles.

higher than the theoretical capacity of graphite (372 mAh g^{-1}). Moreover, the capacity retention of the sample is excellent: the capacity assessed during the second $0.7 \mu\text{A cm}^{-2}$ measurement almost recovered to that assessed during the first $0.7 \mu\text{A cm}^{-2}$ measurement. Thus, we have demonstrated the LIB anode operation of the MLG formed at low temperature (350°C).

4. Conclusions

To fabricate a carbon anode for flexible rechargeable batteries, we developed a low-temperature (350°C) self-organization process of the anode electrode structure, consisting of MLG/metal/plastic, using a Ni-induced LE technique. The MLG anode shows excellent characteristics as a low-temperature formed MLG. This study contributes to the development of flexible rechargeable batteries with reliable carbon anodes.

References

- [1] H. Murata, *et al.*, *JJAP*, **56**, 05DE03 (2017).
- [2] H. Murata, *et al.*, *ACS Appl. Mat. Interface* **10**, 41664 (2018).
- [3] H. Murata, *et al.*, *APL*, **110**, 033108 (2017).
- [4] H. Murata, *et al.*, *APL*, **111**, 243104 (2017).
(Highlighted by Nature INDEX in March 2018.)
- [5] H. Murata, *et al.*, E-MRS Fall Meeting 2018. (Invited)
- [6] H. Murata, *et al.*, *SciRep*, **9**, 4068 (2019).
(Top 100 downloaded physics papers for SR. in 2019.)
- [7] H. Murata, *et al.*, *ACS Omega*, **4**, 14251 (2019).
- [8] H. Murata, *et al.*, *APEX*, **13**, 055502 (2020).
- [9] H. Murata, *et al.*, *CrystEngComm*, **22**, 3106 (2020).